Simulation of deterministic energy-balance particle agglomeration in turbulent liquid-solid flows (EP)

Derrick O. Njobuenwu (iD), and Michael Fairweather

COLLECTIONS

(EP) This paper was selected as an Editor's Pick
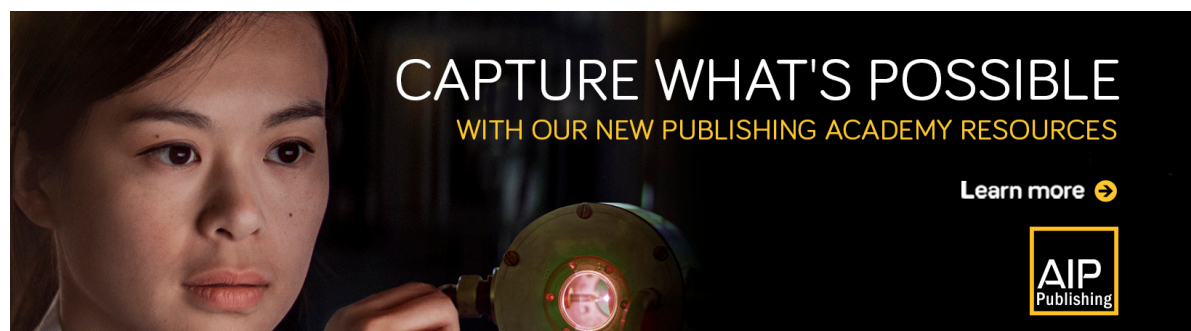
View Online   Export Citation   CrossMark

ARTICLES YOU MAY BE INTERESTED IN

The behaviour of the scalar gradient across the turbulent/non-turbulent interface in jets
Physics of Fluids **29**, 085106 (2017); https://doi.org/10.1063/1.4997951

On the effect of laterally varying boundary heat flux on rapidly rotating spherical shell convection
Physics of Fluids **29**, 086602 (2017); https://doi.org/10.1063/1.4998716

Effects of orthogonal rotating electric fields on electrospinning process
Physics of Fluids **29**, 082003 (2017); https://doi.org/10.1063/1.4997086

AIP Publishing

Simulation of deterministic energy-balance particle agglomeration in turbulent liquid-solid flows

Derrick O. Njobuenwu and Michael Fairweather
School of Chemical and Process Engineering, University of Leeds, Leeds LS2 9JT, United Kingdom

An efficient technique to simulate turbulent particle-laden flow at high mass loadings within the four-way coupled simulation regime is presented. The technique implements large-eddy simulation, discrete particle simulation, a deterministic treatment of inter-particle collisions, and an energy-balanced particle agglomeration model. The algorithm to detect inter-particle collisions is such that the computational costs scale linearly with the number of particles present in the computational domain. On detection of a collision, particle agglomeration is tested based on the pre-collision kinetic energy, restitution coefficient, and van der Waals' interactions. The performance of the technique developed is tested by performing parametric studies on the influence of the restitution coefficient ($e_n = 0.2, 0.4, 0.6,$ and 0.8), particle size ($d_p = 60, 120, 200,$ and $316 \ \mu$m), Reynolds number ($Re_\tau = 150$, 300, and 590), and particle concentration ($\alpha_p = 5.0 \times 10^{-4}$, 1.0×10^{-3}, and 5.0×10^{-3}) on particle-particle interaction events (collision and agglomeration). The results demonstrate that the collision frequency shows a linear dependency on the restitution coefficient, while the agglomeration rate shows an inverse dependence. Collisions among smaller particles are more frequent and efficient in forming agglomerates than those of coarser particles. The particle-particle interaction events show a strong dependency on the shear Reynolds number Re_τ, while increasing the particle concentration effectively enhances particle collision and agglomeration whilst having only a minor influence on the agglomeration rate. Overall, the sensitivity of the particle-particle interaction events to the selected simulation parameters is found to influence the population and distribution of the primary particles and agglomerates formed. *Published by AIP Publishing.* [http://dx.doi.org/10.1063/1.4997089]

I. INTRODUCTION

Of particular interest in this work are the turbulent liquid-solid suspensions encountered in nuclear waste sludge transport and separation processes, where high mass loading is desirable to minimise waste volumes, as well as in many other engineering processes. High particle concentrations with volume fractions over a tenth of a percent result in particle-particle collisions becoming an important physical mechanism[1] in addition to the strong hydrodynamic interactions between the particles and the fluid, although only a fraction of the collisions lead to agglomeration, known as the collision efficiency or agglomeration rate.[2,3] In the reverse process, agglomerates can also be broken-up into smaller particles due to agglomerate-agglomerate or primary particle-agglomerate collisions, through impact with a wall or due to hydrodynamic shear forces in the flow.[4,5] In physical space, the agglomeration and breakup processes occur concurrently. Since breakup is a secondary process succeeding the earlier agglomeration process, the rate of breakup will depend on the population and structural dimension of agglomerates in the system. Hence, the balance between agglomeration and breakup events controls the instantaneous particle size distribution. It is therefore important to understand the underlying physics of particle interactions encountered in systems and equipment processing fluids populated with cohesive particles and for which, in many situations, agglomeration represents an operational problem.

Undertaking studies on the hydrodynamic transport of suspended particles, taking into account their physicochemical behaviour using physical modelling of particle interactions in turbulence, is a difficult task, even with current technologies. One of the challenges with physical modelling of particle-particle interactions (collision and agglomeration events) is in the difficulties encountered in undertaking well-controlled experiments where individual effects can be isolated from others and investigated in detail. The alternative to physical modelling is the use of computational fluid dynamic (CFD) approaches, which require accurate treatment of the carrier and dispersed phases as well as interphase interactions.

Particle agglomeration is affected by the interplay between two physically independent processes, manifested in two distinct steps:[6] the transport step, governed by the hydrodynamic transport of particles, and the attachment step, where inter-particle collisions and physicochemical interactions between two bodies result in the colliding particles either sticking together or bouncing off one another.[7,8] These steps leading to agglomeration have long been used in the framework of fouling studies. However, the transport and attachment steps occur at different scales (time and space) and have often been studied separately by researchers with interests in fluid mechanics, hydrodynamics, and the surface and interface sciences.

Two main approaches exist for treating particle-laden turbulent flows, namely, the Eulerian-Eulerian approach where both the carrier phase and the dispersed phase are

computed in an Eulerian framework, and the Eulerian-Lagrangian approach in which the carrier phase is again calculated on an Eulerian basis and the dispersed phase is treated as Lagrangian markers.[9] Here, an Eulerian-Lagrangian approach is adopted because it gives detailed information about every particle's position, force, and velocity and since this method allows more flexibility in treating particle agglomeration and agglomerate breakup in a turbulent flow. The carrier phase is predicted by the use of numerical resolution of only the largest and most energetic turbulent eddies, with sub-grid scale modelling of the small scales, i.e., using large-eddy simulation (LES). The motion of the dispersed phase is computed using a discrete particle simulation taking into account all the significant hydrodynamic forces acting on a particle. When particles are in close proximity, they may collide and subsequently agglomerate.

There are two common approaches to simulating inter-particle collision: time-driven simulation (also known as the soft-sphere model or discrete element method)[10] and event-driven simulation (also known as the hard-sphere model).[11–15] Besides the soft- and hard-sphere collision models, a stochastic collision detection model has also been developed and extensively applied by Sommerfeld and co-workers.[2,16] This paper adopts the hard-sphere collision model, which has been applied in the simulation of two- and three-phase channel and pipe flows,[12–15] to treat the hydrodynamic transport of particles. Predicting particle agglomeration is achieved by extending the hard-sphere model to handle cohesion. Three common extensions and their variants exist for treating the attachment step:[17] the energy-based agglomeration model,[2,18–20] the momentum-based model,[3,14,20–22] and the energy barrier approach based on DLVO interactions[7] (named after the work of Derjaguin and Landau,[23] and Verwey and Overbeek[24]).

We have adopted the energy-balance agglomeration model which has been successfully applied by Sommerfeld and co-workers.[2,16] Jürgens[18] included oblique collisions to the energy based agglomeration model allowing relative tangential velocities at the contact point. Alletto[19] extended the energy-balance agglomeration model to account for friction at the contact point, allowing the translational and rotational kinetic energies of the particles to be accommodated in the energy balance and the resulting agglomeration process. The energy-based agglomeration model of Alletto[19] was further improved and validated by Breuer and Almohammed[21] and Almohammed and Breuer[20] who provided a detailed validation of the agglomeration model and considered the sensitivity of agglomeration to selected simulation parameters. This model and its variants have successfully been applied to study particle agglomeration in laminar and turbulent flows of various complexities.[3,14,18–21,25–27]

There is also insufficient literature on the effect of various physical and flow properties of the fluid and particles in simulations of particle transport and interactions in turbulent flow. The work described in this paper is, therefore, intended to extend the current literature[2,3,20,21] on the sensitivity of particle-particle interactions to both particle physical properties and flow properties, and specifically, covers values of the latter not considered previously. The present work is undertaken using high-resolution large-eddy simulations

and a hard-sphere, energy-based agglomeration model in a Lagrangian framework using a four-way coupled approach. The simulations are performed in a turbulent channel flow at varying shear Reynolds numbers and at a particle volume fraction that ensures four-way coupling between the fluid and the dispersed phase.

The paper is organised as follows. In Sec. II, we describe the predictive approaches used in this work covering simulation of the continuous and dispersed phases, together with the methods employed to handle particle-particle interactions and cohesion, and their coupling. In Sec. III, relevant results obtained in our simulations are given and discussed. Finally, the main findings are summarised and conclusions are drawn in Sec. IV.

II. NUMERICAL METHODOLOGY

A. Continuous phase

An LES solver, BOFFIN (Boundary Fitted Flow Integrator),[28] was used to compute fully developed turbulent channel flows at shear Reynolds numbers $Re_\tau = u_\tau h/\nu = 150$, 300, and 590, where u_τ is the shear velocity, ν is the fluid kinematic viscosity, and h is the channel half-height. In the present study, we consider water with density $\rho = 1000$ kg m^{-3} and kinematic viscosity $\nu = 1.0 \times 10^{-6}$ m^2 s^{-1}. The size of the channel domain, the number of grid points used, and the filter widths employed are summarised in Table I, together with similar values for the direct numerical simulations (DNS) used for validation. Periodic boundary conditions are imposed along the homogeneous directions, i.e., the spanwise (y-axis) and streamwise (z-axis), and no-slip conditions are used at the walls.

The BOFFIN code implements Cartesian velocity components and a boundary conforming general curvilinear coordinate system with a co-located variable storage arrangement. It is based on a fully implicit low Mach number formulation and is second order accurate in space and time. For the momentum equation convection terms, an energy-conserving discretisation scheme is used. All other spatial derivatives are approximated by standard second-order central differences. Time derivatives are approximated by a three-point backward

TABLE I. Grid parameters for LES of turbulent channel flow. $L_{x(y,z)}$, $N_{x(y,z)}$, and $\Delta^+_{x(y,z)}$ are the size of the domain, the number of grid points, and the filter widths in wall units, respectively. Grid parameters used for DNS at $Re_\tau = 150$ by Marchioli *et al.*,[29] $Re_\tau = 300$ by Marchioli and Soldati,[30] and $Re_\tau = 590$ by Moser *et al.*[31] are also provided for reference.

Re_τ	$L_x \times L_y \times L_z$	$N_x \times N_y \times N_z$	Δ^+_x	Δ^+_y	Δ^+_z
		Current LES			
150	$2h \times 2\pi h \times 4\pi h$	$129 \times 128 \times 128$	0.07–7.10	7.42	14.84
300	$2h \times 2\pi h \times 4\pi h$	$129 \times 128 \times 128$	0.14–14.2	14.84	29.68
590	$2h \times 2\pi h \times 4\pi h$	$129 \times 128 \times 128$	0.26–26.39	29.19	58.38
		DNS			
150	$2h \times 2\pi h \times 4\pi h$	$129 \times 128 \times 128$	0.05–3.68	7.42	14.84
300	$2h \times 2\pi h \times 4\pi h$	$257 \times 256 \times 256$	0.02–3.68	7.39	14.78
590	$2h \times \pi h \times 2\pi h$	$257 \times 384 \times 384$	0.04–7.20	4.80	9.70

difference scheme with a variable time step to ensure that the maximum Courant number, based on the filtered velocity, always lies between 0.1 and 0.2. A two-step, second-order, time-accurate approximate factorisation method is applied to determine the pressure and ensure mass conservation in conjunction with a Rhie and Chow[32] pressure smoothing technique to prevent even-odd node uncoupling of the pressure and velocity fields. The system of algebraic equations resulting from the discretisation is solved using the matrix preconditioned conjugate gradient method BI-CGSTAB[33] for the matrix of velocity vectors, and ICCG[34] for the pressure. This LES solver has been validated thoroughly for many different flows, e.g., Refs. 28 and 35.

BOFFIN solves the space-filtered mass and momentum conservation equations for an incompressible fluid, with the contributions of the dispersed phase being regarded as point sources of momentum,

$$\frac{\partial \bar{u}_j}{\partial x_j} = 0, \tag{1}$$

$$\frac{\partial \bar{u}_i}{\partial t} + \bar{u}_j \frac{\partial \bar{u}_i}{\partial x_j} = -\frac{1}{\rho}\frac{\partial \bar{p}}{\partial x_i} + \frac{\partial}{\partial x_j}\bar{\sigma}_{ij} - \frac{\partial}{\partial x_j}\tau_{ij} + \frac{\Pi_i}{\rho} + \frac{\bar{S}_{m,i}}{\rho}, \tag{2}$$

where $\bar{\sigma}_{ij} = -2\nu\bar{S}_{ij}$ represents the viscous stress, $\bar{S}_{ij} = \frac{1}{2}(\partial \bar{u}_i/\partial x_j + \partial \bar{u}_j/\partial x_i)$ is the filtered strain-rate tensor, $\tau_{ij} = \overline{u_i u_j} - \bar{u}_i \bar{u}_j$ is the sub-grid scale (SGS) tensor which represents the effect of the SGS motions on the resolved motions, t is the time, x_j is the spatial coordinate directions, u_j is the velocity vector, p is the pressure, and ρ is the density. The SGS tensor is computed using the dynamic version of the Smagorinsky model proposed by Piomelli and Liu,[36] with its detailed implementation presented in a recent paper.[35] The filter width Δ is taken as the cube root of the local grid cell volume, $\Delta = (\Delta_x\Delta_y\Delta_z)^{1/3}$. In Eq. (2), $\Pi_3 = -\rho u_\tau^2/h$ is the constant mean pressure imposed along the streamwise direction (z-axis) that drives the flow. $S_{m,i}$ is a source term and accounts for the action of the particles on the fluid, given by the sum of all hydrodynamic forces in the momentum equation of all particles in a fluid computational cell. Further details of the LES approach may be found elsewhere.[28,35]

During particle motion, particle-turbulence interactions occur in which the particles are dispersed by the turbulence of the continuous phase, and the turbulence of that phase is modulated by the presence of the particles. The characteristics of these interactions are accounted for by the momentum exchange between the fluid and the dispersed particles through the momentum term, Eq. (3), which is added as a source term to the fluid Navier-Stokes equation,

$$\bar{S}_{m,i=x,y,z} = -\frac{1}{\Delta^3}\sum_{\alpha=1}^{n_p}\left(m_p\frac{dv_i}{dt}\right), \tag{3}$$

where n_p is the number of particles present in a particular cell volume and m_p is the mass of each particle in the cell.

B. Dispersed phase

The motion of a particle in an LES-predicted turbulent flow field can be viewed as a random process, with its position determined by a deterministic part, evaluated in terms of filtered values, and a stochastic component, arising from the SGS turbulent motions of the fluid phase. For a liquid-solid flow, the hydrodynamic forces (drag, shear lift, pressure gradient, and added mass) are considered, and a stochastic Markov model[28] is used to represent the influence of the unresolved carrier fluid velocity fluctuations experienced by a stochastic particle over a time interval dt which is added to the deterministic contribution,

$$\mathbf{dv} = \left\{\frac{(\bar{\mathbf{u}} - \mathbf{v})}{\tau_p}f_D + C_{SL}\frac{3}{4}\frac{\rho}{\rho_p}\left[(\bar{\mathbf{u}} - \mathbf{v})\times\bar{\boldsymbol{\omega}}\right] + \frac{\rho}{\rho_p}\frac{D\bar{\mathbf{u}}}{Dt}\right.$$
$$\left. + \frac{1}{2}\frac{\rho}{\rho_p}\left(\frac{d\bar{\mathbf{u}}}{dt} - \frac{d\mathbf{v}}{dt}\right)\right\}dt + \left(C_o\frac{k_{sgs}}{\tau_t}\right)^{0.5}\mathbf{dW_t}, \tag{4}$$

$$\mathbf{dx}_p = \mathbf{v}\,dt, \tag{5}$$

where a boldfaced type denotes a matrix-vector and the terms on the right-hand side of Eq. (4) are, respectively, contributions from the drag, shear lift, pressure-gradient, and added mass forces, and the SGS fluid velocity fluctuations.[28] Gravity and buoyancy forces were not included as the focus was limited to turbulence effects on agglomeration events. The history force term was also neglected in the force balance for particle motion due to its arguably weak effect when compared to the drag force term,[37] and in addition due to difficulties in its implementation and computational cost. The particle properties are denoted by the subscript p, and fluid properties are either given without subscript (for readability) or by the subscript f (where it enhances clarity). $\mathbf{v}$ and $\mathbf{x_p}$ are the particle instantaneous velocity and position; $\bar{\mathbf{u}}$ and $\bar{\boldsymbol{\omega}} = 0.5(\nabla\times\bar{\mathbf{u}})$ are known resolved fluid velocities and rotation interpolated at particle position. The expression $f_D = 1.0 + 0.15Re_p^{0.687}$, taken from the Schiller and Naumann drag correlation, is a nonlinear correction term and is applied when a particle's dynamic Reynolds number $Re_p = |\bar{\mathbf{u}} - \mathbf{v}|d_p/\nu$ is large and the Stokes flow paradigm becomes invalid, with d_p being the particle diameter. $\tau_p = \Phi_p d_p^2/(18\nu)$ is the particle relaxation time and, when normalised by the viscous time scale $\tau_f = \nu/u_\tau^2$, gives the particle Stokes number, $\tau_p^+ = \tau_p/\tau_f$, which is then used to characterise the particle response time, with $\Phi_\rho = \rho_p/\rho$ being the particle to fluid density ratio. Hence, a superscript ($^+$) denotes the variables made dimensionless in wall (viscous) units using the fluid kinematic viscosity, ν, and the fluid shear velocity, u_τ. The shear lift force coefficient C_{SL} accounts for corrections due to small and large particle Reynolds numbers as proposed by Mei[38] and applied by Njobuenwu et al.[9] The time derivative $D\mathbf{u}/Dt = \partial\mathbf{u}/\partial t + \mathbf{u}\cdot\nabla\mathbf{u}$ is the fluid acceleration as observed at the instantaneous particle position.

The stochastic term [last term in Eq. (4)] consists of a model constant C_0 taken as unity and the SGS turbulence kinetic energy, k_{sgs}, which accounts for the effects of the SGS stresses on particle dispersion through the use of the Wiener process $d\mathbf{W_t}$. The SGS kinetic energy is obtained using equilibrium arguments from $k_{sgs} = 2\Delta C_s^{2/3}\bar{S}_{ij}\bar{S}_{ij}$, where Δ is the filter width and C_S is the dynamically calibrated Smagorinsky parameter. During a simulation, the increment of the Wiener process, $\Delta\mathbf{W_t}$, is represented by $\Delta W_{t,i} = \xi_i\times\Delta t$, where ξ_i is a random vector sampled with zero mean and a variance of unity, determined independently for each time step. The interaction

between particles and the fluid phase turbulence is taken into account by the time scale $\tau_t = \tau_p$, with other alternative time scales given in Bini and Jones.[28]

The effect of particle rotation and the corresponding lift force due to such rotation can be predicted by solving for the angular velocity of the particles and modelling the torque exerted on them through correlations similar to the drag laws. Although neglected in the present work, this could potentially impact on the particle volume fraction field and inter-particle collisions. However, without these rotational effects, the pointwise formulation of particle transport employed predicts the particle evolution in qualitative agreement with approaches accounting for particle rotation. The neglect of such rotation at this stage of development would, therefore, appear warranted, although it will be considered in future work.

C. Particle-particle interactions

The particle-particle interactions involve inter-particle collisions and the agglomeration of collided particles.

1. Deterministic collision algorithm

The deterministic hard sphere collision model was implemented subject to some assumptions:

(1) Particles and agglomerates are modelled as spheres, and interaction between the particles is due to binary collisions.
(2) Collision is frictionless, and particle angular momentum is not considered.
(3) Only small deformations of particles are allowed post-collision.

In modelling the particle binary collisions, the likely collision partners are first identified by a deterministic method where, for small time steps, only collisions between neighbouring particles are likely. By using the concept of virtual cells (e.g., Refs. 13 and 26), the cost of checking for collisions can be reduced from $O(N_0^2)$, when collisions between all possible particle pairs are considered, to $O(N_0)$ by dynamically adjusting the virtual cell during the simulation to an optimum size such that the number of particles per cell is sufficiently low, with the size user-specified.[26] With high particle volume fractions $\alpha_p > 10^{-3}$ in the system and $N_0 \sim O(10^6$–$10^8)$, the use of virtual cells in reducing the computational cost of checking for collisions from $O(N_0^2)$ to $O(N_0)$ is a significant advantage when adopting this technique for industrial flows. The computational domain is first decomposed into virtual cells. For a near optimal virtual cell size, d^n is dynamically adjusted during the simulation in order to limit the maximum number of particles in the cell, $N_{p,\max}^0$, with this number specified as an input to the CFD code. The optimum value for the factor d^n is given by following the work of Alletto,[19]

$$d^n = d^{n-1} \left(N_{p,\max}^0 / N_{p,\max}^{n-1} \right)^{-1/3}, \quad (6)$$

where d^{n-1} is the factor used to decompose the computational domain at the previous time step $(n-1)$, and $N_{p,\max}^0$ and $N_{p,\max}^{n-1}$ are the maximum number of particles allowed

to be contained in a virtual cell and the maximum number of particles found in one of the virtual cells at the previous time step, respectively. An optimum value for $N_{p,\max}^0$ for particle-particle collisions in a turbulent channel flow has been found to be within the range 10–100.[19] Hence, a value of $N_{p,\max}^0 = 25$ was adopted for the simulations reported in this paper, used to allow a compromise between high accuracy and efficiency in the handling of particle-particle collisions. All particles within the same virtual cell are tagged by the same index.

Consequently, collision detection procedures are limited to the particles in each virtual cell using a hard-sphere collision model similar to that described in Refs. 12, 13, 15, and 26. In the interests of brevity, the details of this classical deterministic collision detection algorithm will be not repeated here, and readers are referred to Refs. 12, 13, 15, and 26 for further details.

2. Energy balance agglomeration model

The attachment step succeeds the collision step, subject to the following assumptions:

(1) In a typical waste sludge,[39] the particles are in contact with highly alkaline and high ionic strength salt solutions, where the electrical double layer associated with charged sites on particle surfaces collapses, and electrostatic repulsions that can disperse particles of like charge are inhibited. Hence, only van der Waals' force components of the DLVO theory are responsible for post-collision cohesion.
(2) Agglomeration is based on the pre-collision energy balance and van der Waals' interactions.
(3) The agglomerate size and structure are based on a volume-equivalent sphere.
(4) Particles are assumed to agglomerate if the cohesive force exceeds the segregation force, otherwise, they separate.

Agglomeration of the colliding particles is based on an expression which permits agglomeration if the elastic energy (i.e., the relative kinetic energy before the collision minus the dissipated energy) after the compression period of the collision is less than the work required to overcome van der Waals' forces,[19]

$$\frac{\left(\mathbf{v_2^-} - \mathbf{v_1^-} \right)^2 - \left[\left(\mathbf{v_2^-} - \mathbf{v_1^-} \right) \cdot \mathbf{n_c} \right]^2 \left(1 - e_n^2 \right)}{\left| \left(\mathbf{v_2^-} - \mathbf{v_1^-} \right) \cdot \mathbf{n_c} \right|}$$
$$\leq \frac{H^*}{6\delta_0^{*2}} \left[\left(1 - e_n^2 \right) \frac{6}{\pi^2 \rho_p^* \bar{\sigma}^*} \frac{d_{p,1}^{*3} + d_{p,2}^{*3}}{d_{p,1}^{*2} d_{p,2}^{*2} \left(d_{p,1}^* + d_{p,2}^* \right)} \right]^{1/2}, \quad (7)$$

where quantities with the superscript * are dimensionless and are defined as follows: the particle density $\rho_p^* = \rho_p / \rho$, particle diameter $d_p^* = d_p / h$, Hamaker constant $H^* = H/(\rho u_b^2 h)$, and yield pressure $\bar{\sigma}^* = \bar{\sigma}/(\rho u_b^2)$, and where $\delta_0^* = \delta_0 / h$ is the minimal contact distance; u_b is the bulk velocity and h is the channel half-height. Note that the superscript $(-)$ denotes quantities before the collision, and the subscripts 1 and 2 denote particles number one and two. The amount of dissipated energy relative to the incident kinetic energy is

quantified by $(1 - e_n^2)$, in terms of the coefficient of restitution, e_n. The restitution coefficient is not constant but depends on factors such as the initial relative approach speed of the particles, their relative velocities of recession after collision, and the particle material (see, e.g., Ref. 40). The hard-sphere model adopted here, however, treats this coefficient as a constant that can be estimated from empirical investigations. Note that the energy-balance-based agglomeration model, Eq. (7), adopted has been successfully validated against theoretical results for test cases in both laminar and turbulent flow regimes.[19–21] Numerical results obtained using large-eddy simulation were found to be in close agreement with theory, and subsequently, the energy-based model was applied to investigate the dynamic process of particle agglomeration in vertical fully developed turbulent channel and pipe flows using LES.

When Eq. (7) is not fulfilled (i.e., no agglomeration occurs) and hence the particles bounce apart from each other due to the resulting impulse during impact, the velocities and positions of both particles have to be updated according to the following equations:

$$\mathbf{v_1^+} = \mathbf{v_1^-} + \frac{m_{p,2}}{m_{p,1} + m_{p,2}} \left\{ (1 + e_n) \left[\left(\mathbf{v_2^-} - \mathbf{v_1^-} \right) \cdot \mathbf{n_c} \right] \mathbf{n_c} \right\}$$
$$\mathbf{v_2^+} = \mathbf{v_2^-} + \frac{m_{p,1}}{m_{p,1} + m_{p,2}} \left\{ (1 + e_n) \left[\left(\mathbf{v_2^-} - \mathbf{v_1^-} \right) \cdot \mathbf{n_c} \right] \mathbf{n_c} \right\}, \quad (8)$$

$$\mathbf{x_1^+} = \mathbf{x_{1,c}} + (t_{n+1} - t_c)\mathbf{v_1^+}$$
$$\mathbf{x_2^+} = \mathbf{x_{2c}} + (t_{n+1} - t_c)\mathbf{v_2^+}, \quad (9)$$

where $\mathbf{x_{1c}}$ and $\mathbf{x_{2c}}$ denote the coordinates of the centre of mass of particles p_1 and p_2 at the instant of collision, respectively. However, if Eq. (7) holds (i.e., agglomeration occurs) and a volume-equivalent agglomerate structure[2,19,21] is assumed, as is the absence of interstitial space between agglomerated particles with the same density as the primary particles, then conservation of mass is satisfied. The velocity and position of the centre of mass of the agglomerate, p_3, at the end of the current time step are derived based on conservation of the translational momentum of the collision partners,[12]

$$\mathbf{v_3^+} = \frac{\mathbf{v_1^-} d_{p,1}^3 + \mathbf{v_2^-} d_{p,2}^3}{d_{p,3}^3}, \quad (10)$$

$$\mathbf{x_3^+} = \frac{\mathbf{x_{1c}} + \mathbf{x_{2c}}}{2} + (t_{n+1} - t_c)\mathbf{v_3^+}. \quad (11)$$

The diameter of the agglomerate, $d_{p,3}$ in Eq. (10), is obtained from conservation of mass as[12]

$$d_{p,3} = \sqrt[3]{d_{p,1}^3 + d_{p,2}^3}. \quad (12)$$

D. Coupling particle transport, collision, and agglomeration

Coupling the transport and attachment steps is not straightforward. The range of the physicochemical interfacial (DLVO) forces is limited to a few tens of nanometres, a distance much smaller than that of typical particle motion and inter-particle distances in fluids. Following an analogy from Henry et al.,[8] a typical energy barrier which a binary collision needs to overcome to effect agglomeration occurs at separation distances as small as $\Delta x = 3$ nm and, in most cases, the eventual energy barrier is found at distances, for collisions with a wall, that is of the order of $\Delta x = 10$ nm. Taking the lowest shear Reynolds number flow considered, $Re_\tau = u_\tau h/\nu = 150$ ($u_\tau = 7.5 \times 10^{-3}$ m s^{-1}, $\nu = 10^{-6}$ m^2 s^{-1}), the range of DLVO forces in wall units is then typically of the order of $\Delta x_{DLVO}^+ = \Delta x u_\tau/\nu = 7.5 \times 10^{-3}$. This is much smaller than the typical hydrodynamic distance Δx^+ which is equal to the distance travelled by particles in one (hydrodynamic) time step: $\Delta t^+ \sim 1$, $\Delta x^+ = u^+ \times \Delta t^+ \sim 1$. In this case, if one were to choose such a time step and introduce DLVO effects as forces in the particle equation of motion, Eq. (4), the particles would leap over the very narrow range where DLVO forces are significant, thus avoiding the particle-surface interaction altogether,[8] or causing inter-particle penetration or overlap. Alternatively, the fluid time step could be reduced to the range where DLVO forces are significant. However, doing this will result in very expensive simulations as the time interval for a time step will increase by $O(10^3)$. To circumvent the large-scale differences between distances associated with the actions of the DLVO forces, the size of the particles, the hydrodynamic transport of particles, and inter-particle collisions, an efficient modelling approach was adopted such that each step was treated separately during each time step (hydrodynamic transport of particles, inter-particle collision, and cohesion of collided particles). Hence, the coupling of the transport and attachment steps was achieved without drastically reducing the overall time step.

III. RESULTS AND DISCUSSION

A. Fluid velocity fields

A visual impression of the change in the character of the flow field with increasing shear Reynolds number, Re_τ, is given in Fig. 1, where instantaneous cross-sectional snapshots of the streamwise velocity are shown at one streamwise z-position. Note that the fluid flow field predictions reported in this section were obtained using one-way coupling, i.e., $S_{m,i} = 0$ in Eq. (2), with the particle phase non-existent. The general increase in the range of scales present with increasing Reynolds number is evident across the wall-normal direction, although the large scales dominate for all Reynolds numbers in the central region of the channel. El Khoury et al.[41] have reported that the average spacing between near-wall low-speed streaks is approximately one-half and a tenth of the channel half-height for the lowest and highest Re_τ flows considered, respectively. This is in conformity with the observed near-wall flow pattern in Fig. 1(a) for the lowest Re_τ and in Fig. 1(c) for the largest Re_τ.

Simulation results for the fluid phase were monitored for various averaging start times and averaging periods to evaluate when a statistically stationary state and converged statistics for all shear Reynolds number cases were achieved. Figures 2(a), 2(c), and 2(e) show the profile of the mean streamwise velocity, $u_z^+ = \langle u_z \rangle/u_\tau$, in the wall-normal direction, $x^+ = xu_\tau/\nu$, obtained for three shear Reynolds number flows, $Re_\tau = 150$, 300, and 590, giving the resolved velocity.
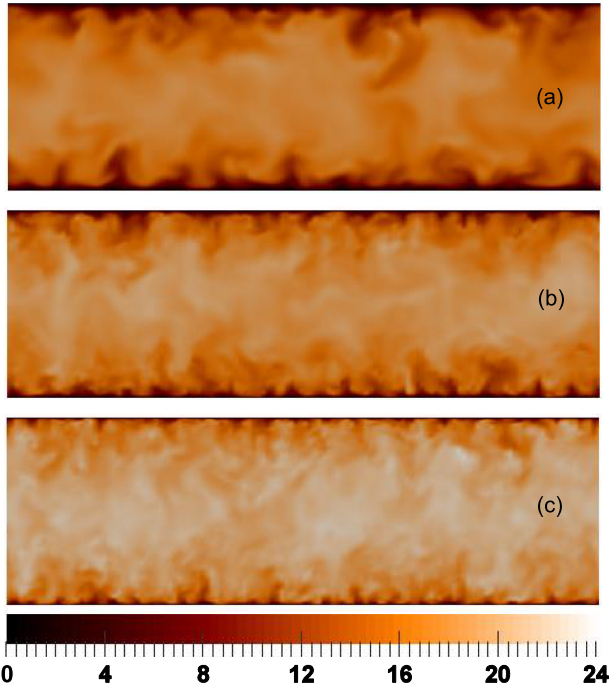
FIG. 1. Instantaneous streamwise velocity field, u_z^+, in the x–y planes at $z^+ = 3000$ for (a) $Re_\tau = 150$, (b) $Re_\tau = 300$, and (c) $Re_\tau = 590$. Contour levels are shown for $0 \leq u_z^+ \leq 24$ from black to white shades.

The corresponding profiles of the root mean square of the fluctuating velocity components in the wall-normal, $u'^+_{x,\text{rms}} = \langle u'_{x,\text{rms}} \rangle / u_\tau$, the spanwise, $u'^+_{y,\text{rms}} = \langle u'_{y,\text{rms}} \rangle / u_\tau$, and the streamwise, $u'^+_{z,\text{rms}} = \langle u'_{z,\text{rms}} \rangle / u_\tau$, directions, and of the shear stress $u'^+_x u'^+_z = \langle u'_x u'_z \rangle / u_\tau^2$, are plotted in Figs. 2(b), 2(d), and 2(f). The LES results are compared with those obtained from the DNS database of Marchioli et al.[29] at a shear Reynolds number, $Re_\tau = 150$, Marchioli and Soldati[30] at $Re_\tau = 300$, and Moser et al.[31] at $Re_\tau = 590$. The comparison shows very good agreement, although the degree of agreement reduces with increasing Re_τ due to the reducing numerical resolution. This agreement confirms that the use of a highly resolved LES and dynamic modelling of the SGS term gives reliable results, with the results for the turbulence stresses at higher Re_τ improved when the unresolved, i.e., SGS, contributions are included in the velocity statistics.

B. Discrete particle simulation

The particle equations of motion were integrated using a fourth-order Runge-Kutta scheme, while a trilinear interpolation scheme[29] was used to obtain the fluid velocity, $\bar{\mathbf{u}}$, SGS kinetic energy, k_{sgs}, and fluid rotation, $\bar{\boldsymbol{\omega}}$, at a particle's position. The particles' initial position, $\mathbf{x}_{\mathbf{p},0}$, at $t^+ = 0$ was random, and the initial velocity was set equal to that of the fluid at the particle's position. For particle-wall interactions, the perfect elastic collision condition was adopted such that all collisions resulted in a rebound back into the computational domain with no loss of kinetic energy. This ideal perfect elastic collision model was adopted to focus our attention on the main scope of the work: the deterministic agglomeration model. Periodic boundary conditions were applied along the homogeneous directions, making it possible to prolong the duration of the flow by continuous "recirculation" of the fluid and particles back into the domain.

Since no DNS-based predictions or experimental data for particle-particle collision and agglomeration at the shear Reynolds numbers of $Re_\tau = 150$, 300, and 590 are available, a one-way coupled simulation was used to validate the discrete particle simulation technique using a suitable reference case. The statistics of inertial particles at nondimensional particle response times $\tau_p^+ = 1$, 5, and 25 are compared with the dispersed phase velocity obtained from the DNS database of Marchioli and Soldati[30] at a shear Reynolds number, $Re_\tau = 300$. The density ratio is set to $\rho_p/\rho \sim 790$, equal to that used in the one-way coupled gas-solid turbulent channel flow DNS of Marchioli and Soldati,[30] in which only the drag force using the Schiller and Naumann drag correlation was considered. From Fig. 3, all the velocity profiles reported for the three particle response times are in very good agreement with the DNS of Marchioli and Soldati.[30] Furthermore, the degree of agreement obtained between the particle mean streamwise velocity and the components of the turbulence intensity reflects the accuracy reported for the single phase velocity statistics in Fig. 2.

C. Particle-particle interactions

Using the algorithms developed in this work, we report the performance of the coupled LES and Lagrangian particle tracker with a deterministic particle-particle interaction model. The sensitivity of particle-particle interactions in a turbulent channel flow to four simulation parameters, namely, the shear Reynolds number, particle size, normal restitution coefficient, and particle volume fraction, is examined. Three flow shear Reynolds numbers, $Re_\tau = 150$, 300, and 590, four particle sizes, $d_p = 60$, 120, 200, and 316, four normal restitution coefficient values, $e_n = 0.2$, 0.4, 0.6, and 0.8, and three particle volume fractions (concentrations), $\alpha_p = 5.0 \times 10^{-4}$, 1.0×10^{-3}, and 5.0×10^{-3}, are examined for a constant density, $\rho_p = 2710$ kg m^{-3}. The density ratio between the particles and the fluid was $\rho_p/\rho = 2.71$. The mechanical properties of the particles and simulation parameters are summarised in Table II. Note that the largest particle size considered, $d_p = 316$ μm, is of the same order as the Kolmogorov length scale in all the flows examined, lying between the smallest and largest values predicted. The particles were introduced into the computational domain after achieving a fully developed single-phase flow field, with a new time counter, $t^+ = t u_\tau^2 / \nu = 0$, initiated at this point after which collision and agglomeration counts were taken. It should also be noted that the particle concentration field was still uniformly distributed and had not reached an asymptotic, statistically stationary stage at the start of sampling of the particle-particle interactions. However, in many practical applications, the particle collision statistics shortly after particle release are of more interest than the asymptotic values.[42]

1. Dependency of particle-particle interactions on restitution coefficient

First, the sensitivity of particle-particle interactions to the normal restitution coefficient, e_n, which denotes the ratio
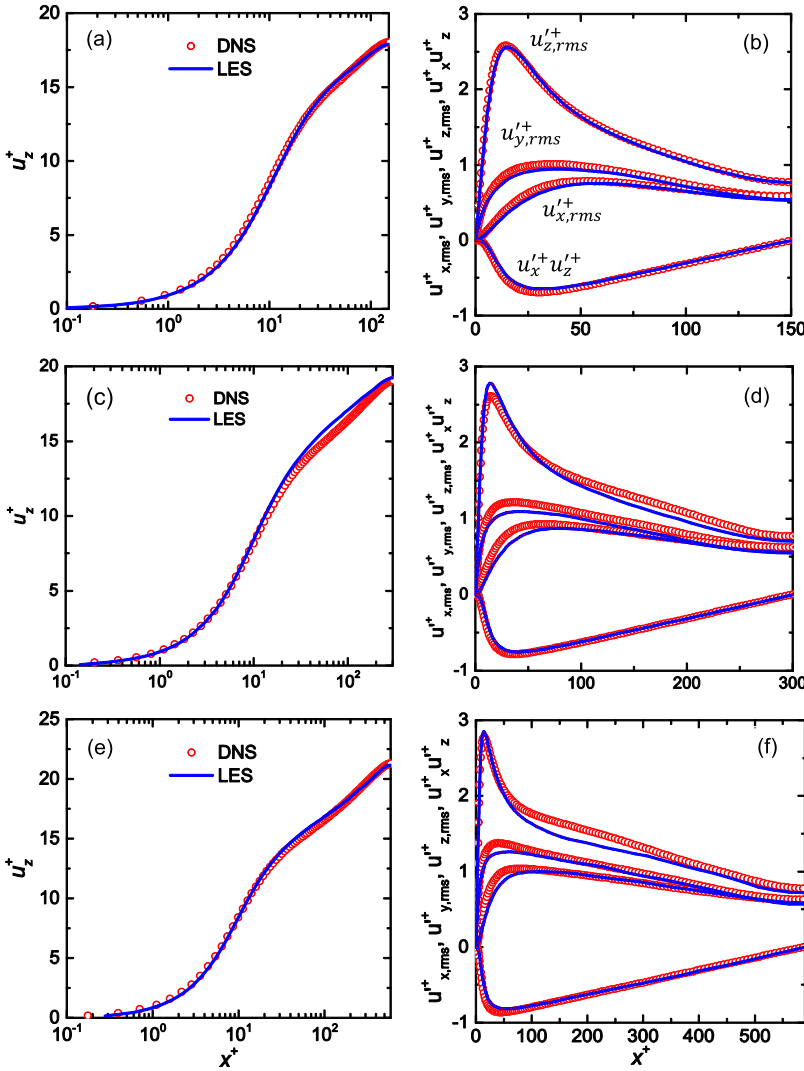
FIG. 2. Statistical moments of the turbulent channel flow: (*left*) mean streamwise velocity, (u_z^+), and (*right*) wall-normal ($u_{x,\mathrm{rms}}'^+$), spanwise ($u_{y,\mathrm{rms}}'^+$), and streamwise ($u_{z,\mathrm{rms}}'^+$) root mean square of velocity fluctuations, and Reynolds shear stress ($u_x'^+ u_z'^+$). [(a) and (b)] $Re_\tau = 150$, [(c) and (d)] $Re_\tau = 300$, and [(e) and (f)] $Re_\tau = 590$.

of the relative velocity before and after collision, is examined. The restitution coefficient can be obtained numerically, analytically, or measured in laboratory experiments and has been reported[2] as $e_n = 0.4$ for calcite, a nuclear waste sludge simulant. The interest in the sensitivity of the agglomeration process to e_n is necessitated due to the scatter in e_n values reported in the literature and the fact that e_n values for the materials and conditions of interest in this work, required as input to the simulations, are not readily available. The normal coefficient of restitution in the particle-particle interaction model controls how much of the kinetic energy remains for the colliding particles to rebound from one another versus how much is dissipated as heat, or work done in deforming the colliding pair. The amount of dissipated energy relative to the incident kinetic energy is quantified by $(1 - e_n^2)$ which appears directly in the agglomeration criterion, Eq. (7), showing that a normal restitution coefficient $e_n = 0$ indicates a complete dissipation of kinetic energy and of relative normal motion, whereas a normal restitution coefficient $e_n > 0$ implies a post-collisional consequence of the particles bouncing off one another or sticking together. For a purely elastic impact with $e_n = 1$, no kinetic energy is dissipated. Hence, an increase in e_n enhances the impulsive force, decreases the

amount of energy dissipated during the collision, and weakens the cohesive force between the colliding particles, thus reducing the probability of agglomeration conditions being satisfied.

Figure 4 shows the time evolution of the effect of the normal coefficient of restitution on the number of the accumulated particle-particle collisions, N_{col}, and the total number of the accumulated particle-particle collisions resulting in agglomeration, N_{agg}, both normalised by the initial total number of primary particles injected, N_0, for a shear Reynolds number, $Re_\tau = 150$, primary particle diameter, $d_p = 60$ μm, and particle volume fraction, $\alpha_p = 1 \times 10^{-3}$. Besides the value of $e_n = 0.4$ reported for calcite,[2] additional values of $e_n = 0.2$, 0.6, and 0.8 are used to investigate the influence of the coefficient of restitution on particle-particle interactions. Note that unless otherwise stated, sampling of the collision and agglomeration events started at the beginning of the simulation, and the results shown here are for simulations run up to dimensionless time $t^+ = 1000$ in wall units. However, the agglomeration process continued beyond this reported time interval.

From Fig. 4, the number of particle collisions, N_{col}, and agglomerations, N_{agg}, varies approximately linearly with time,
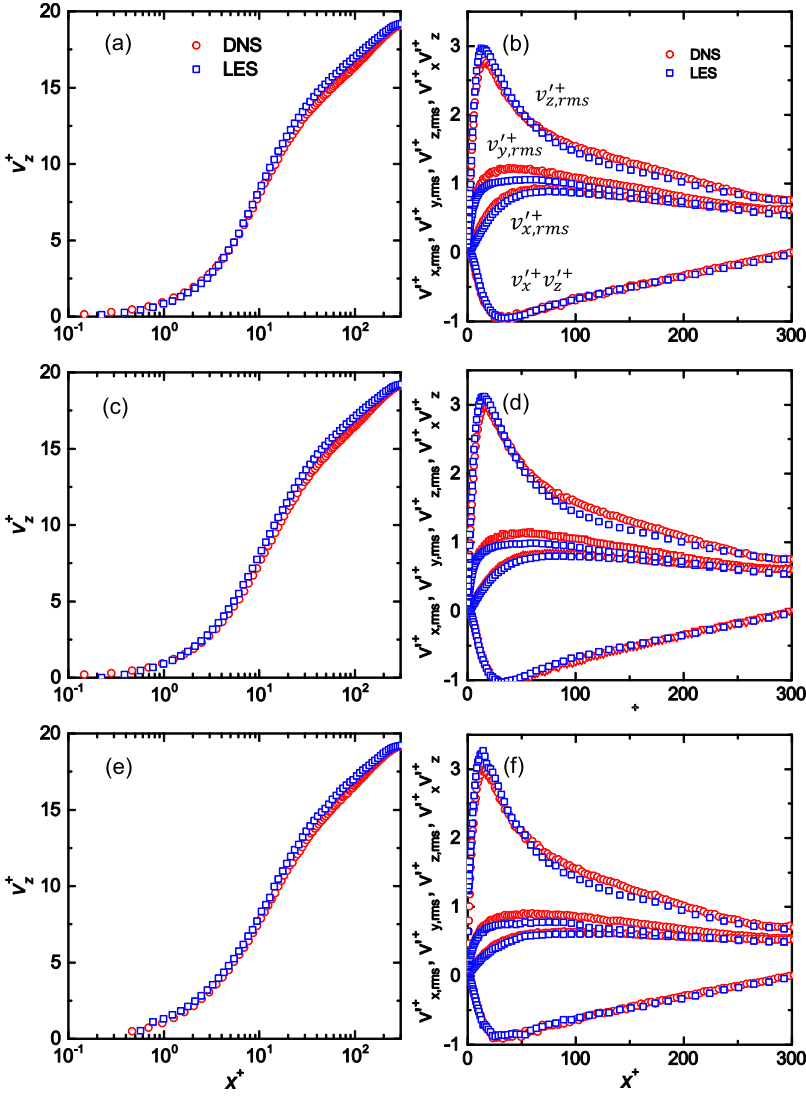
FIG. 3. Statistical moments of particles in the turbulent channel flow for one-way coupled simulation at a particle density ratio, $\rho_p/\rho \sim 790$: (*left*) mean streamwise velocity, (v_z^+), and (*right*) wall-normal ($v'^+_{x,\text{rms}}$), spanwise ($v'^+_{y,\text{rms}}$), and streamwise ($v'^+_{z,\text{rms}}$) root mean square of velocity fluctuations, and Reynolds shear stress ($v'^+_x v'^+_z$). [(a) and (b)] $\tau_p^+ = 1$, [(c) and (d)] $\tau_p^+ = 5$, and [(e) and (f)] $\tau_p^+ = 25$.

t^+, and shows a strong dependence on the particle normal restitution coefficient. The larger the coefficient of restitution, the larger the collision frequency and the smaller the number of such collisions resulting in agglomeration, supporting previous observations.[43] Hence, from Fig. 4, the number of collisions with respect to the normal restitution coefficient at any time has a trend directly opposite to the number of agglomeration processes. This observation slightly differs to that of Breuer and Almohammed[21] who reported that both N_{col} and N_{agg} showed a similar dependency on e_n such that N_{col} and N_{agg} decreased with an increase in e_n. However, predictions of

collision efficiency from previous works[2,19,21] have a similar trend to that of the present predictions, shown in Fig. 5. The disparity between the present results and those reported by Breuer and Almohammed[21] on the influence of e_n on N_{agg}/N_0 is likely due to the difference in the initial conditions adopted for the particle-particle interactions between both sets of simulations.

The collision efficiency (also known as the agglomeration rate), N_{agg}/N_{col}, is defined as the ratio of the total number of accumulated particle-particle collisions leading to agglomeration to the total number of the accumulated particle-particle collisions. Figure 5 shows a sharp change in the profile of N_{agg}/N_{col} from the start of the simulations to around $t^+ \sim 100$, which then remains relatively constant up to $t^+ \sim 200$. Beyond $t^+ \sim 200$, N_{agg}/N_{col} slightly increases with time. This increase with time beyond $t^+ \sim 200$ is caused by the initial conditions adopted for the particle-particle interactions which also led to the disparity between values for N_{agg}/N_0 given in Fig. 4 and those reported in Breuer and Almohammed.[21]

Additional insights into the influence of the normal restitution coefficient on particle-particle interactions in a turbulent channel flow for the base case ($Re_\tau = 150$, $d_p = 60$ μm, $\alpha_p = 1 \times 10^{-3}$) can be obtained from the results of Fig. 6.

TABLE II. Particle mechanical properties and simulation parameters.

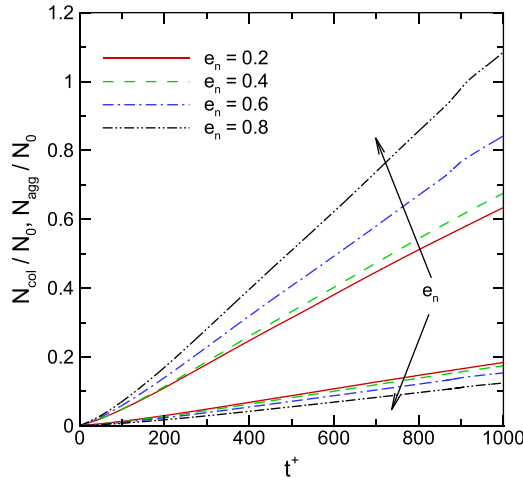| Parameter	Symbol	Unit	Value
Density	ρ_p	kg m^{-3}	2710
Hamaker constant	H	J	3.8×10^{-20}
Mean yield stress	σ	Pa	3.0×10^{8}
Minimal contact distance	δ_0	m	2.0×10^{-10}
Diameter	d_p	μm	60, 120, 200, 316
Normal restitution coefficient	e_n	...	0.2, 0.4, 0.6, 0.8
Particle volume fraction	α_p	...	5×10^{-4}, 1×10^{-3}, 5×10^{-3}

FIG. 4. Distribution of the total number of particle-particle collision events, N_{col}, and the total number of particle-particle collisions leading to agglomeration, N_{agg}, normalised by the initial total number of primary particles, N_0, as a function of the non-dimensional simulation time, t^+, for various values of the normal coefficient of restitution, e_n ($Re_\tau = 150$, $d_p = 60\,\mu$m, $\alpha_p = 1 \times 10^{-3}$, upper curves N_{col}/N_0, lower curves N_{agg}/N_0).
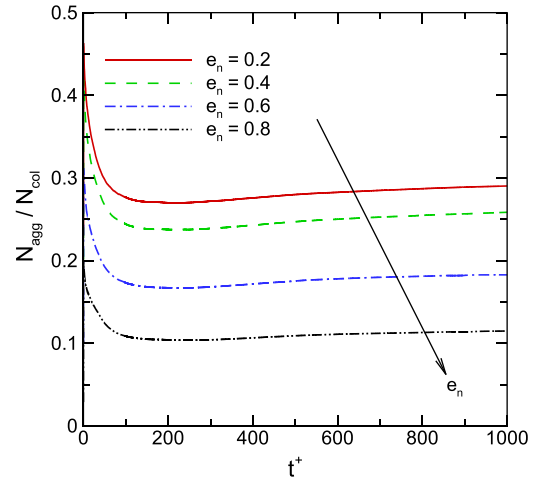

FIG. 5. Distribution of the agglomeration rate, N_{agg}/N_{col}, as a function of the non-dimensional simulation time, t^+, for various values of the normal coefficient of restitution, e_n ($Re_\tau = 150$, $d_p = 60\,\mu$m, $\alpha_p = 1 \times 10^{-3}$).

Figure 6(a) shows the time evolution of the total number of the agglomerated primary particles (i.e., the total number of the primary, or single, particles involved in all agglomerates), N_{pp}. As observed by Breuer and Almohammed,[21] the results demonstrate that although more agglomerates are formed with time, the number of agglomerated primary particles decreases with an increase in the normal restitution coefficient. This observation of N_{pp} decreasing with an increase in e_n is expected as fewer agglomerates are formed at higher e_n, as discussed in relation to Figs. 4 and 5. The total number of agglomerates (multiple particles, excluding single particles), N_a, irrespective of the agglomerate type (or size), over time is shown in Fig. 6(b). Similar to the observations from Fig. 6(a), the total number of agglomerates formed increases with time and is inversely proportional to the value of the normal restitution coefficient.

Figure 7(a) shows the average number of primary particles included in an agglomerate, defined as the ratio of the total number of agglomerated primary particles, N_{pp}, to the total number of agglomerates, N_a, and its variation with dimensionless time, t^+. These results again illustrate that the size of the agglomerates with respect to the number of primary particles included in the agglomerate increases with a decrease in the normal restitution coefficient. This is again expected and, with respect to Figs. 4–6, a large e_n favours a post-collisional state of particles bouncing off one another whilst a small e_n encourages particles involved in binary collisions to stick together. Within the time interval reported, up to $t^+ \sim 1000$, the average number of primary particles included in an agglomerate, N_{pp}/N_a, falls within the double and triple particle agglomerate range as $N_{pp}/N_a \sim 2$–3. From the onset of agglomerates being formed from a population of single particles, the value of N_{pp}/N_a is about 2 as the double particles are the first agglomerate size to be formed. As the simulation time progresses, most of the double particles already formed combine with other agglomerates or singles to form agglomerates of higher size, hence, the average value N_{pp}/N_a shifts away from 2 towards 3, as is evident in Fig. 7(a). This is because the lesser multiple particle agglomerates are more readily formed than larger agglomerates. The precursors for the formation of two and three particle agglomerates are the single particles, and they have the largest number density within the time interval reported, as will be shown later in Fig. 8.

Furthermore, and again as will be shown later, collision and agglomeration processes are strongly dependent on the size of the two particles involved in any particle-particle interaction. More collisions and subsequent agglomerations, therefore, take place the smaller the particle size. Figure 7(b) compares the number of primary particles [i.e., single (1)] and agglomerates of the same type [double (2), triple (3), quadruple (4), quintuple (5), sextuple (6), etc., particles] formed after a simulation time $t^+ = 1000$ for the four normal restitution
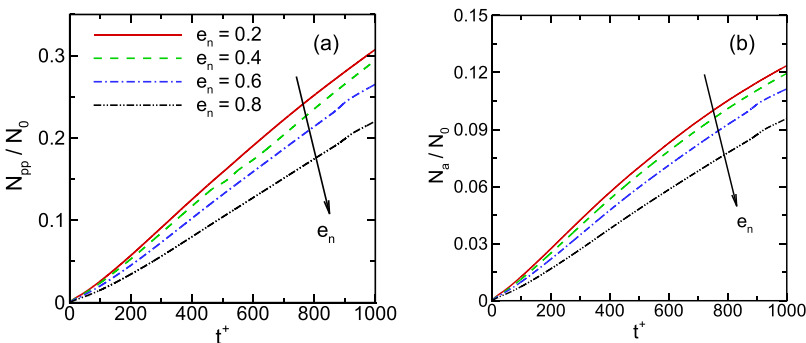

FIG. 6. Influence of the normal restitution coefficient, e_n, for particle-particle interaction on the time evolution of (a) the total number of the agglomerated primary particles, N_{pp}, and (b) the total number of agglomerates, N_a, both normalised by the initial total number of primary particles, N_0 ($Re_\tau = 150$, $d_p = 60\,\mu$m, $\alpha_p = 1 \times 10^{-3}$).
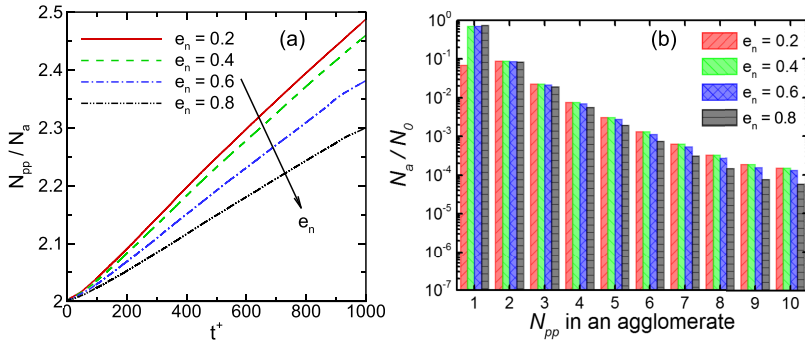
FIG. 7. Influence of the normal restitution coefficient, e_n, for particle-particle interaction on (a) the time evolution of the average number of primary particles included in an agglomerate, N_{pp}/N_a, and (b) the number of particles or agglomerates of the same type [single (1), double (2), triple (3), quadruple (4), etc., particles] after a simulation time, $t^+ = 1000$ ($Re_\tau = 150$, $d_p = 60 \ \mu$m, $\alpha_p = 1 \times 10^{-3}$).

coefficients ($e_n = 0.2$, 0.4, 0.6, and 0.8) investigated. For the agglomerate sizes reported, an increase in e_n produces a larger population of single particles, but with a reduction, in general, in the number of agglomerates of the same size, a trend also observed by Breuer and Almohammed.[21] The size of the agglomerates in terms of the number of primary particles included in the agglomerate, N_{pp}, generally increases with a decrease in the normal restitution coefficient, particularly for agglomerates with up to ten primary particles. Further simulation time would allow agglomerates made up of more than ten primary particles to be considered, although clear trends can be established over the total simulation time considered, making longer run times unnecessary.

Figure 8 shows the population balance (growth and/or death) of the single and multi-sized particle agglomerates, defined as the percentage of the ratio of the number of particle sizes to the initial number of total single particles, after a simulation time $t^+ = 1000$. The results of Fig. 8 complement the earlier observations noted in regard to Fig. 7. Figure 8 therefore demonstrates that an increase in e_n decreases the rate of depletion of the primary particles, such that at any given time the number of single particles in the system increases and the size of the various agglomerates, in terms of the number of primary particles included in the agglomerate, decreases with increasing e_n, as was observed by Breuer and Almohammed.[21]

Overall, the notable feature in Figs. 4–8 is the strong dependence of particle-particle interactions on the coefficient of restitution, e_n, with a summary of key simulation parameters at the dimensionless time $t^+ = 1000$ given in Table III. Increasing e_n from 0.2 to 0.8 has a dramatic effect on the parameters reported, such that N_{col}/N_0 increases from 0.634 to 1.086 showing a linear proportionality, N_{agg}/N_0 diminishes from 0.184 to 0.125 implying an inverse relationship, and N_{agg}/N_{col} decreases from 0.290 to 0.115, again suggesting an inverse dependence. Others parameters such as N_{pp}/N_0 reduce from 0.307 to 0.220, N_a/N_0 decrease in value from 0.124 to 0.096, while N_{pp}/N_a reduce from 2.488 to 2.300, demonstrating that agglomeration-related parameters generally depend strongly on e_n in an inverse fashion. One obvious feature of the results is therefore that the larger the coefficient of restitution, e_n, the larger the number of collision events, N_{col}, and the smaller the value of the agglomeration events, N_{agg}, N_{agg}/N_{col}, N_a, and N_{pp}.

2. Effect of particle size on particle-particle interactions

Particle size has an influence on the value of the two forces on both sides of the agglomeration equation, Eq. (7). Particle size (or inertia) has therefore been shown to have a significant influence on the relative velocity between the two particles. Agglomeration occurs when the attractive forces are predominant; and the smaller the particle size is, the higher these forces are, as is evident in Eq. (7). Hence, agglomeration processes are sensitive to the size of the primary particles. Lin and Wey[44] reported that the tendency for particles to agglomerate is proportional to the surface area of the particles. Small particles have a larger surface area per unit volume, thereby favouring agglomeration.
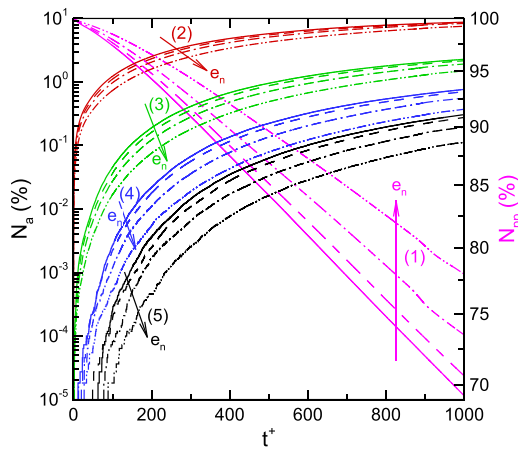

FIG. 8. Influence of the normal restitution coefficient, e_n, for particle-particle interaction on the time evolution of the population of single and multiple particles. Line numbers: single (1), double (2), triple (3), quadruple (4), quintuple (5) ($Re_\tau = 150$, $d_p = 60 \ \mu$m, $\alpha_p = 1 \times 10^{-3}$).

TABLE III. Values of particle-particle collisions (N_{col}/N_0), agglomeration events (N_{agg}/N_0), agglomeration rate (N_{agg}/N_{col}), agglomerated primary particles (N_{app}/N_0), agglomerate number (N_a/N_0), and average number of primary particles included in an agglomerate (N_{pp}/N_a) for different normal restitution coefficients, e_n, after a dimensionless time $t^+ = 1000$ ($Re_\tau = 150$, $d_p = 60 \ \mu$m, $\alpha_p = 1 \times 10^{-3}$).

e_n	N_{col}/N_0	N_{agg}/N_0	N_{agg}/N_{col}	N_{pp}/N_0	N_a/N_0	N_{pp}/N_a
0.2	0.634	0.184	0.290	0.307	0.124	2.488
0.4	0.676	0.175	0.258	0.294	0.119	2.460
0.6	0.842	0.154	0.183	0.265	0.111	2.382
0.8	1.086	0.125	0.115	0.220	0.096	2.300

In order to investigate the effect of particle size on particle-particle interaction processes, it is necessary that the global particle volume fraction, α_p, and not the number of primary particles, N_0, be comparable. N_0 values used in the simulations were 75 250 for $d_p = 316$ μm particles, increasing to 10 992 290 for $d_p = 60$ μm particles. Since the N_0 values used for the four particle sizes ($d_p = 60, 120, 200,$ and 316 μm) simulated are not comparable, the particle-particle interaction parameters have to be normalised by N_0 for comparisons to be based on a unit particle. The four particle sizes examined can alternatively be organised according to the values of their Stokes number, $\tau_p^+ = \tau_p u_\tau^2 / \nu$. The equivalent Stokes numbers of the four particle sizes are $\tau_p^+ = 3.62 \times 10^{-2}$, 1.45×10^{-1}, 4.02×10^{-1}, and 1.0, respectively. Figure 9 addresses the effects of particle size d_p (or inertia τ_p^+) on collision and agglomeration behaviour in a turbulent channel flow. Figures 9(a)–9(c) show semi-logarithmic plots of the evolution of the normalised total number of particle-particle collision events, N_{col}/N_0, the normalised total number of particle-particle collisions leading to agglomeration, N_{agg}/N_0, and the agglomeration rate (N_{agg}/N_{col}), respectively, as a function of the size of the primary particles, d_p. For these simulations, a normal restitution coefficient $e_n = 0.4$ for calcite, a shear Reynolds number $Re_\tau = 150$, and an initial global volume fraction $\alpha_p \sim 1 \times 10^{-3}$ were used.

It is clearly demonstrated, from the results presented in Figs. 9(a)–9(c), that the collision frequency, N_{col}/N_0, the collision efficiency, N_{agg}/N_0, and the agglomeration rate, N_{agg}/N_{col}, all decrease with an increase in particle size, d_p. These results are in qualitative agreement with theory and with observations reported elsewhere.[2,17,21,45,46] According to theory,[17,46] the kinetic energy between colliding coarse particles is high, whilst that between fine and coarse particles is slightly less, and that between fine particles is the lowest. In contrast to the kinetic energy between particles, the

cohesion energy between small particles is larger than that between coarse particles. However, the sticking behaviour of two individual particles depends on the relative value of the cohesion energy and the kinetic energy between them, as represented in the agglomeration model, Eq. (7). Particles rebound if the kinetic energy is higher than the cohesion energy, while they agglomerate if the inverse is true. Reddy and Mahapatra[45] observed that agglomeration in a fluidised bed combustion power plant takes place when the coal material contains either too many fine particles or coarse particles, or both in very large proportions. The results of Wang *et al.*[17] complemented the latter authors' observations, finding that compared with coarse particles, small particles lead to agglomeration much more readily, and the agglomeration of small particles, or small and coarse particles, is the main mechanism by which agglomeration occurs. Numerical experiments based on full DLVO theory agree with the present results on the sensitivity of particle-particle interactions to the particle size. The DLVO theory, therefore, predicts a marked increase of the total interaction energy with an increase in particle size, and therefore a dramatic decrease in the rate of aggregation of colloidal particles.[7] Hence, the high number of inter-particle collisions, N_{col}/N_0, with reducing particle size, d_p, in Fig. 9(a) is a prerequisite for the large number of agglomeration processes, N_{agg}/N_0, in Fig. 9(b), assuming that the cohesive force is large enough with reducing particle size. The influence of particle size on the number of agglomerates of the same type (double, triple, quadruple, etc.) and the number of non-agglomerated primary particles (single) is shown in Fig. 9(d). After the referenced simulation time, $t^+ \sim 1000$, the smallest particles with $d_p = 60$ μm have undergone more agglomeration processes than the other sizes of particles; hence, there is a smaller number of single particles present in the computational domain, followed by the $d_p = 120, 200,$ and 316 μm particle sizes. Within this time frame, the number of agglomerates, N_a/N_0, of the
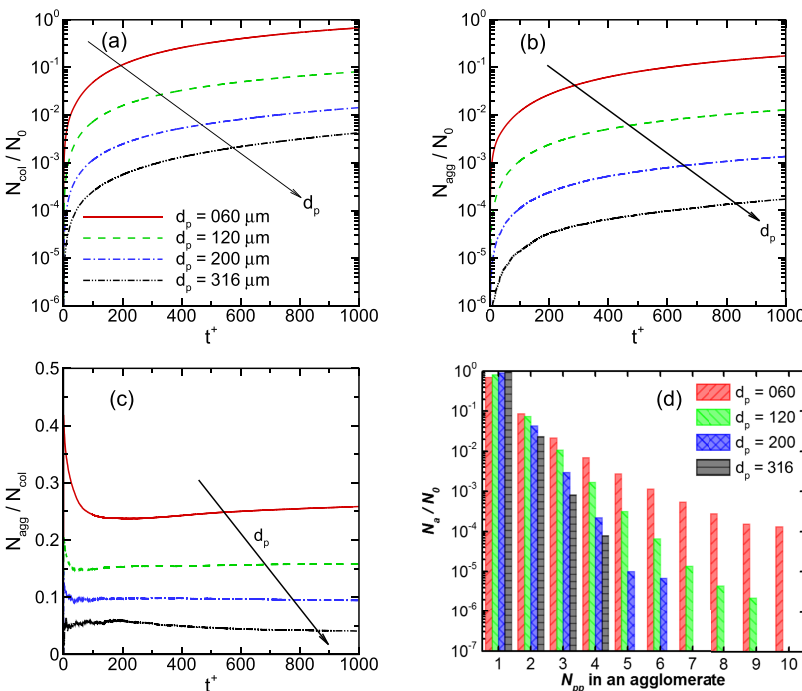
FIG. 9. Distribution of the (a) total number of particle-particle collision events, N_{col}, (b) total number of particle-particle collisions leading to agglomeration, N_{agg}, both normalised by initial total number of primary particles, N_0, (c) agglomeration rate, N_{agg}/N_{col}, all as a function of non-dimensional simulation time, t^+, and (d) number of particles or agglomerates, N_a/N_0, of the same type [single (1), double (2), triple (3), quadruple (4), etc., particles] after a simulation time, $t^+ = 1000$ ($d_p = 60, 120, 200,$ and 316 μm, $Re_\tau = 150$, $e_n = 0.4$, $\alpha_p = 1 \times 10^{-3}$).

TABLE IV. Values of particle-particle collisions (N_{col}/N_0), agglomeration events (N_{agg}/N_0), agglomeration rate (N_{agg}/N_{col}), agglomerated primary particles (N_{app}/N_0), agglomerate number (N_a/N_0), and average number of primary particles included in an agglomerate (N_{pp}/N_a) for different particle sizes after a dimensionless time $t^+ = 1000$ ($Re_\tau = 150$, $e_n = 0.4$, $\alpha_p = 1 \times 10^{-3}$).

$d_p/(\mu m)$	τ_p^+	N_{col}/N_0	N_{agg}/N_0	N_{agg}/N_{col}	N_{pp}/N_0	N_a/N_0	N_{pp}/N_a
60	3.62×10^{-2}	0.676	0.175	0.258	0.294	0.119	2.460
120	1.45×10^{-1}	0.654	0.103	0.158	0.191	0.088	2.177
200	4.02×10^{-1}	0.532	0.050	0.094	0.097	0.047	2.074
316	1.0	0.620	0.025	0.041	0.050	0.024	2.040

same type decreases with an increase in the particle size. This observation complements the earlier finding from the results given in Figs. 9(a)–9(c) that the rate of inter-particle collision and agglomeration decreases as the particle size increases. Hence, only primary particle sizes $d_p = 60$ and 120 μm formed agglomerates with a primary particle number N_{pp} beyond six, whilst only the $d_p = 60$ μm primary particles generated agglomerates with up to 10 constituents.

This relationship between particle-particle interaction and particle size, summarised in Table IV, is as earlier stated and is generally ascribed to the fact that smaller particles have an increased total surface area which leads to more contact, and a higher probability of collision, between particles as compared to their coarser counterparts. As the primary particle size, d_p, increases from 60 to 316 μm, the simulated number of inter-particle collisions, N_{col}/N_0, decreases from 0.675 to 0.532, the number of agglomeration processes, N_{agg}/N_0, reduces from 0.175 to 0.025, and the agglomeration rate, N_{agg}/N_{col}, diminishes from 0.258 to 0.041 by the end of the simulations at time $t^+ = 1000$, all showing an inverse proportionality dependence. It is, therefore, reasonable to infer that smaller particles promote inter-particle collisions and the formation of agglomerates.

3. Effect of shear Reynolds number on particle-particle interactions

Another important parameter that influences particle-particle interactions is the fluid inertia, measured by the flow shear Reynolds number, Re_τ. Note that the effect of different flow Reynolds numbers on particle-particle interactions is equivalent to investigating the impact of turbulence, or fluid velocity, on the same particle-particle interactions. Hence, with other parameters being invariant, the fluid, and by extension, the particle, velocity both have a linear relationship with the flow Reynolds number. It is also important to further note that turbulence-induced agglomeration is commonly categorised into two mechanisms, namely, turbulent fluctuations that cause relative motion between particles (the turbulent transport effect) and the preferential concentration that leads to a highly intermittent local pair density distribution and thus an additional enhancement of the average collision rate (the accumulation effect).[42] The effects of both mechanisms on particle-particle interactions were considered as a whole and not individually.

The sensitivity of particle-particle interactions to the flow shear Reynolds number for a given fixed particle Stokes number, $\tau_p^+ = 1.0$, is shown in Fig. 10. A change in the flow Reynolds number alters the fluid velocities seen by the particles as well as the particles' velocities. With an increase in flow velocity, the ratio of the particle relative kinetic energy to that of the cohesive force is also affected. For fixed particle inertia, measured by its Stokes number, the number of inter-particle collisions in Fig. 10(a) and the number of collisions leading to agglomeration in Fig. 10(b) both show a strong sensitivity to the flow shear Reynolds number. On the other hand, the agglomeration rate in Fig. 10(c) shows a weak dependence on the flow inertia. Increasing the flow shear Reynolds number shows an increase in the normalised number of the
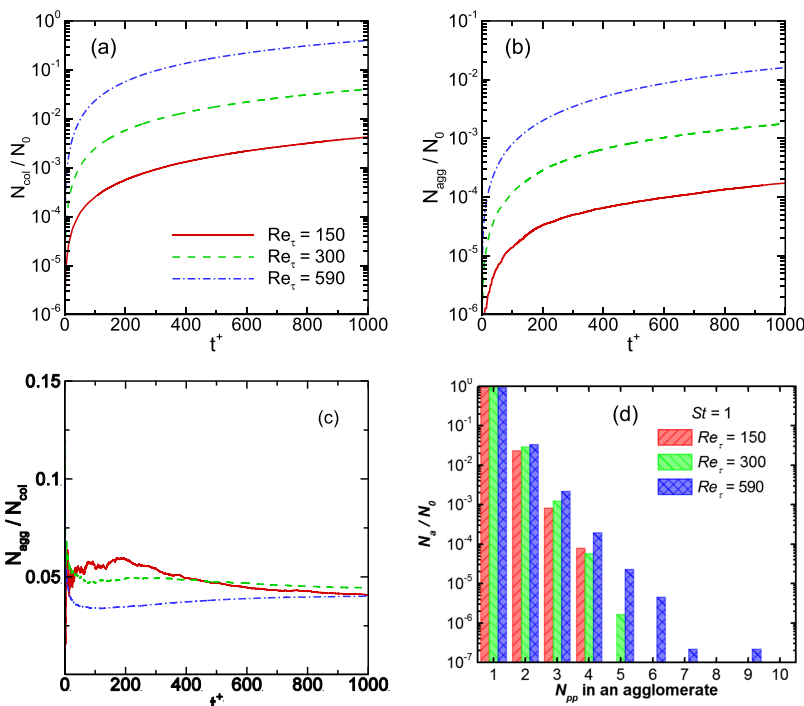

FIG. 10. Distribution of the (a) total number of particle-particle collision events, N_{col}, (b) total number of particle-particle collisions leading to agglomeration, N_{agg}, both normalised by the initial total number of primary particles, N_0, (c) agglomeration rate, N_{agg}/N_{col} all as a function of non-dimensional simulation time, t^+, and (d) number of particles or agglomerates, N_a/N_0, of the same type [single (1), double (2), triple (3), quadruple (4), etc., particles] after a simulation time $t^+ = 1000$ ($Re_\tau = 150$, 300, and 590, particle Stokes number $\tau_p^+ = 1$, $e_n = 0.4$, $\alpha_p = 1 \times 10^{-3}$).

particle-particle collision, N_{col}/N_0, in Fig. 10(a) and an increase in the normalised number of collisions leading to agglomeration, N_{agg}/N_0, in Fig. 10(b). However, the agglomeration rate, N_{agg}/N_{col}, in Fig. 10(c) shows an inverse proportionality with a stronger dependence on the shear Reynolds number at early simulation times. The relationship between N_{agg}/N_{col} and Re_τ becomes weaker as time progresses due to the particle concentration becoming more developed. The relative number of single and multiple particle agglomerates present in the computational domain at the end of the simulation at $t^+ = 1000$ is shown in Fig. 10(d) when the primary particle Stokes number is fixed at $\tau_p^+ = 1.0$. This demonstrates (although difficult to see from the plot) that the relative number of single particles remaining at the end of the simulation is reduced as the shear Reynolds number is increased from $Re_\tau = 150$ to $Re_\tau = 590$. This means that the ratio of the total number of single particles involved in forming agglomerates to the initial number of single particles input to the computational domain, N_a/N_0, is smallest for the lowest shear Reynolds number case. This behaviour corroborates that found in the results of Figs. 10(b) and 10(c) where fewer collisions result in agglomeration, the lower the shear Reynolds number. In terms of the agglomerates, Fig. 10(d) shows that an increasing number of double and triple particle agglomerates occur as the shear Reynolds number increases from $Re_\tau = 150$ to 590. Beyond the triple particle agglomerates, no clear relationship between the agglomerate particle number and Re_τ is evident, with the maximum agglomerate size formed at the end of the simulation consisting of nine primary particles for the $Re_\tau = 590$ case. Agglomerates of five particles and beyond were not found for the lowest shear Reynolds number case, whilst only agglomerates consisting of up to five particles were observed for the moderate shear Reynolds number, $Re_\tau = 300$.

Table V shows that at the end of the investigated simulation time $t^+ = 1000$, as the flow shear Reynolds number Re_τ increases from 150 to 590, for a fixed primary particle Stokes number $\tau_p^+ = 1$, the normalised number of inter-particle collisions, N_{col}/N_0, increases from 0.620 to 0.958, and the normalised number of agglomeration processes, N_{agg}/N_0, increases from 0.025 to 0.038, again showing an inverse proportionality dependence. In contrast, the agglomeration rate, N_{agg}/N_{col}, remains roughly constant over all Re_τ. It can, therefore, be inferred that the Reynolds number has a minimal effect on the formation of agglomerates. Further analysis would, however, be beneficial in reaching conclusions regarding the

influence of the flow Reynolds number on particle collision and agglomeration given that the results considered are influenced by the initial conditions adopted in their simulation.

4. Correlation between degree of particle-particle interactions and particle concentration

The particle volume, α_p, is a dimensionless number that represents the particle concentration in a particle-laden flow. The results of Figs. 11(a) and 11(b) suggest that there exists a strong correlation between the number of particle-particle collisions, N_{col}/N_0, and agglomerations, N_{agg}/N_0, and the particle volume fraction, while in Fig. 11(c), a weak relationship between the agglomeration rate, N_{agg}/N_{col}, and the particle volume fraction is exhibited. As shown in Fig. 11(a), the normalised accumulated number of particle collisions continuously increases with increasing simulation time, t^+, while the number of collisions increases with the particle volume fraction. This trend is consistent with theory as well as with the observations of Ernst and Sommerfeld[47] where the average distance between particles and computed collision times decreased with increasing volume fraction, consequently increasing the probability of the particles being close enough to cause collisions. As for the agglomeration rate, N_{agg}/N_{col}, it can be seen from Fig. 11(c) that its particle volume fraction dependence is weak as the difference in the agglomerate rate with time is similar both in trend and in magnitude, irrespective of the volume fraction, similar to the observations of Ho and Sommerfeld[2] and Balakin *et al.*[3] After an initial instability in the value of N_{agg}/N_{col} due to the evolving particle concentration distribution, the agglomeration rate shows a roughly constant profile with time, with the case with the largest volume fraction, $\alpha_p = 5 \times 10^{-3}$, having the highest agglomerate rate at all times reported. However, in comparison to the results reported by Ho and Sommerfeld[2] and Balakin *et al.*,[3] the case with the largest volume fraction, $\alpha_p = 5 \times 10^{-3}$, in Fig. 11(c) is expected to show the lowest agglomeration rate, N_{agg}/N_{col}. This disparity between N_{agg}/N_{col} in the present and previous results[2,3] is because our largest volume fraction predictions may still be influenced by their initial conditions. For cases with higher volume fraction, therefore, the flow needs more time to reach a statistically steady state owing to the large number of inter-particle collisions. The two cases with lower volume fractions, $\alpha_p = 5 \times 10^{-4}$ and $\alpha_p = 1 \times 10^{-3}$, show no significant differences in the magnitude of the agglomeration rate after the initial settling period but follow the expected trend in which the $\alpha_p = 1 \times 10^{-3}$ case shows a slightly higher agglomeration rate than the $\alpha_p = 5.0 \times 10^{-4}$ case towards the end of the simulation where the particles have reached a statistical steady state. Overall, the profiles shown in Figs. 11(a)–11(c) demonstrate that the rate of normalised particle collisions, in Fig. 11(a), and the normalised agglomeration rate, in Fig. 11(b), are similar in terms of their ratio, as given in Fig. 11(c). As expected, the results of Fig. 11(d) indicate that the depletion of the primary single particles at the end of the simulation, $t^+ = 1000$, is highest for the very concentrated case, $\alpha_p = 5 \times 10^{-3}$, with this depletion decreasing with particle volume fraction. The same reasoning given in relation to the results of Figs. 11(a) and 11(b) applies here. In terms of the number of multiple particle agglomerates present

TABLE V. Values of particle-particle collisions (N_{col}/N_0), agglomeration events (N_{agg}/N_0), agglomeration rate (N_{agg}/N_{col}), agglomerated primary particles (N_{app}/N_0), agglomerate number (N_a/N_0), and average number of primary particles included in an agglomerate (N_{pp}/N_a) for different shear Reynolds numbers Re_τ after a dimensionless time $t^+ = 1000$ ($\tau_p^+ = 1$, $e_n = 0.4$, $\alpha_p = 1 \times 10^{-3}$).

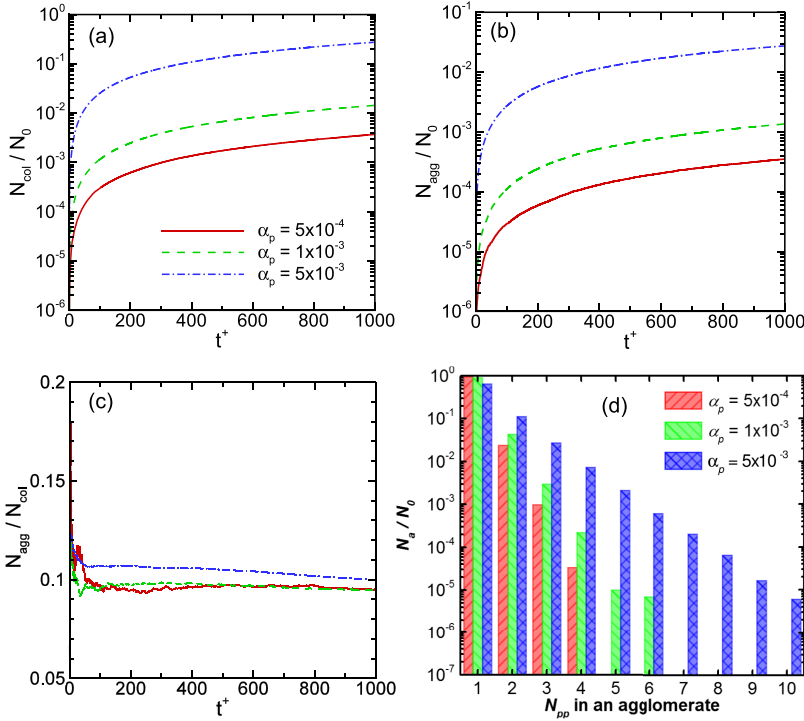| Re_τ	$d_p/(\mu m)$	N_{col}/N_0	N_{agg}/N_0	N_{agg}/N_{col}	N_{pp}/N_0	N_a/N_0	N_{pp}/N_a
150	316	0.620	0.025	0.041	0.050	0.024	2.040
300	158	0.730	0.032	0.044	0.063	0.031	2.044
590	80.25	0.958	0.038	0.040	0.074	0.036	2.074

FIG. 11. Distribution of the (a) total number of particle-particle collision events, N_{col}, (b) total number of particle-particle collisions leading to agglomeration, N_{agg}, both normalised by the initial total number of primary particles, N_0, (c) agglomeration rate, N_{agg}/N_{col}, all as a function of non-dimensional simulation time, t^+, and (d) number of particles or agglomerates, N_a/N_0, of the same type [single (1), double (2), triple (3), quadruple (4), etc., particles] after a simulation time, $t^+ = 1000$ ($Re_\tau = 150$, particle Stokes number $\tau_p^+ = 1$, $e_n = 0.4$, $\alpha_p = 5 \times 10^{-4}$, 1×10^{-3}, and 5×10^{-3}).

at the end of the simulation, a linear dependency is evident between the number of agglomerates of a particular type and the volume fraction. The higher the concentration, the more the agglomeration, and the larger the number of agglomerates of a particular type present in the computational domain. Hence, the case with the highest particle volume fraction, $\alpha_p = 5 \times 10^{-3}$, shows the largest number of agglomerates of all types, followed by the moderate and then lowest concentration cases. Only agglomerates of up to six and four particles are formed at the end of the simulation for cases with particle volume fractions of $\alpha_p = 1 \times 10^{-3}$ and $\alpha_p = 5 \times 10^{-4}$, respectively, due to the slower collision and agglomeration rates in these cases.

Lastly, Table VI gives the numerical values of the various collision and agglomeration parameters considered in Fig. 10 at the end of the simulation for the case involving a shear Reynolds number, $Re_\tau = 150$, particle normal restitution coefficient, $e_n = 0.4$, and primary particle size, $d_p = 60 \ \mu$m. Here, the correlation between the degree of particle-particle interactions and agglomerations, and the particle concentration, as noted above, is again clear.

TABLE VI. Values of particle-particle collisions (N_{col}/N_0), agglomeration events (N_{agg}/N_0), agglomeration rate (N_{agg}/N_{col}), agglomerated primary particles (N_{app}/N_0), agglomerate number (N_a/N_0), and average number of primary particles included in an agglomerate (N_{pp}/N_a) using different fractal dimensions after a dimensionless time $t^+ = 1000$ ($Re_\tau = 150$, $d_p = 60 \ \mu$m, $\alpha_p = 1 \times 10^{-3}$).

α_p	N_{col}/N_0	N_{agg}/N_0	N_{agg}/N_{col}	N_{pp}/N_0	N_a/N_0	N_{pp}/N_a
5×10^{-4}	0.274	0.026	0.095	0.050	0.025	2.042
1×10^{-3}	0.634	0.184	0.290	0.307	0.124	2.488
5×10^{-3}	0.842	0.154	0.183	0.265	0.111	2.382

IV. CONCLUSIONS AND OUTLOOK

An efficient CFD model has been described and used to advance our understanding of particle-particle interactions (collision and agglomeration events) in turbulent flows, augmenting the limited amount of work performed in this area to date. The developed method combines an Eulerian-Lagrangian technique, and deterministic hard sphere collision and energy balance agglomeration models, in the context of large-eddy simulation. The LES predicted flow field has been found to be in very good agreement with single-phase flow results obtained from direct numerical simulations of $Re_\tau = 150$, 300, and 590 channel flows. In addition, the discrete particle simulation technique described in this paper has been successfully validated using DNS of a $Re_\tau = 300$ gas-solid flow. The present contribution has focused on the dependency of particle-particle interactions in a turbulent channel flow on the particle normal restitution coefficient, e_n, particle size (diameter, d_p, and Stokes number, τ_p^+), flow shear Reynolds number, Re_τ, and particle volume fraction, α_p. Although the results of the simulations studied in this work lack any direct quantitative comparison with physical measurements, they do lead to qualitative explanations and insights into the particle-particle interactions occurring in a wall-bounded turbulent flow.

The results demonstrated that the normalised number of particle collisions, N_{agg}/N_0, and the agglomeration process, N_{agg}/N_0, vary linearly with time, t^+, and are strongly dependent on the particle normal restitution coefficient, e_n. The larger the coefficient of restitution, the larger the number of collisions (N_{col}/N_0), the smaller the number of such collisions resulting in agglomeration (N_{agg}/N_0), and the smaller the agglomeration rate (N_{agg}/N_{col}), supporting previous observations.[20,21,43] It should be noted that in reality, the coefficient of restitution will be a function, amongst other things, of the

particle impact velocity, and hence it would be more appropriate to employ a dynamic value rather than the range of constant values employed herein. Clearly, the present results demonstrate the strong dependence of particle-particle interactions on this coefficient. Based on the current observations, however, it can be inferred that for a dynamic coefficient of restitution, as a function of the particle impact velocity, the trends observed should be maintained while the magnitude of those trends may be altered. Future work will consider the use of such a dynamic coefficient.

Particle-particle interactions are also sensitive to the primary particle size (characterised by its diameter, d_p) or the particle inertia (characterised by its Stokes number, τ_p^+), the flow inertia (characterised by the flow shear Reynolds number, Re_τ), and the particle concentration (characterised by the particle volume fraction, α_p). The relationship between particle size and particle-particle interactions shows an inverse proportionality. By analysing the particle-particle interaction events of primary particles with different sizes, it is concluded that the normalised collision frequency, N_{col}/N_0, collision efficiency, N_{agg}/N_0, and agglomeration rate, N_{agg}/N_{col}, all decrease with an increase in particle size, d_p. Again, this effect of particle size on particle-particle interactions is consistent with, and complements, that reported elsewhere.[2,3,17] Increasing the flow shear Reynolds number, Re_τ, from 150 to 590 showed an increase in N_{col}/N_0, and an increase in N_{agg}/N_0, whereas N_{agg}/N_{col}, showed an inverse proportionality with, and stronger dependency on, the shear Reynolds number. An increase in the particle volume fraction, α_p, from $\alpha_p = 5 \times 10^{-4}$ to $\alpha_p = 5 \times 10^{-3}$, leads to a decrease in the space between two particles within a flow and their time between collisions, which effectively enhances particle collision and agglomeration. However, the particle volume fraction has only a minor influence on the collision efficiency, although an inverse proportionality is evident, notwithstanding the anomalous trend exhibited by the $\alpha_p = 5 \times 10^{-3}$ case whose initial conditions are still persistent because the flow required more time to reach a statistically steady state due to the large number of collisions. Overall, the sensitivity of particle-particle interaction events to the selected simulation parameters subsequently influenced the population and distribution of the primary single particles and multiple particle agglomerates formed.

The deterministic agglomeration model formulated and used in this work, although relatively simple, possesses the qualitative, and to a lesser degree, the quantitative features required to explain experimentally observed behaviour of agglomeration processes. Lastly, it should be noted that the results presented were derived by monitoring particle-particle interactions immediately following the injection of particles into the flow. This initial condition was used consistently and represents only one of the number of initial conditions that have been used in studies of particle-laden flows. As such, however, the flows may not have attained a statistically steady state in some situations, and it is expected that the initial conditions would have exerted some influence on selected cases, as already mentioned within the text. Further work will explore the influence of such conditions on the conclusions reached above.

[1] S. Elghobashi and G. C. Truesdell, "On the two-way interaction between homogeneous turbulence and dispersed solid particles. I: Turbulence modification," Phys. Fluids **5**, 1790 (1993).

[2] C. A. Ho and M. Sommerfeld, "Modelling of micro-particle agglomeration in turbulent flows," Chem. Eng. Sci. **57**, 3073 (2002).

[3] B. Balakin, A. C. Hoffmann, and P. Kosinski, "The collision efficiency in a shear flow," Chem. Eng. Sci. **68**, 305 (2012).

[4] Y. Ammar, A. Dehbi, and M. W. Reeks, "Break-up of aerosol agglomerates in highly turbulent gas flow," Flow Turbul. Combust. **89**, 465 (2012).

[5] M. U. Babler, L. Biferale, L. Brandt, U. Feudel, K. Guseva, A. S. Lanotte, C. Marchioli, F. Picano, G. Sardina, A. Soldati, and F. Toschi, "Numerical simulations of aggregate breakup in bounded and unbounded turbulent flows," J. Fluid Mech. **766**, 104 (2015).

[6] C. Henry, J.-P. Minier, M. Mohaupt, C. Profeta, J. Pozorski, and A. Tanière, "A stochastic approach for the simulation of collisions between colloidal particles at large time steps," Int. J. Multiphase Flow **61**, 94 (2014).

[7] C. Henry, J.-P. Minier, J. Pozorski, and G. Lefèvre, "A new stochastic approach for the simulation of agglomeration between colloidal particles," Langmuir **29**, 13694 (2013).

[8] C. Henry, J.-P. Minier, and G. Lefèvre, "Towards a description of particulate fouling: From single particle deposition to clogging," Adv. Colloid Interface Sci. **185-186**, 34 (2012).

[9] D. O. Njobuenwu, M. Fairweather, and J. Yao, "Coupled RANS–LPT modelling of dilute, particle-laden flow in a duct with a 90° bend," Int. J. Multiphase Flow **50**, 71 (2013).

[10] P. A. Cundall and O. D. L. Strack, "A discrete numerical model for granular assemblies," Géotechnique **29**, 47 (1979).

[11] B. P. B. Hoomans, J. A. M. Kuipers, W. J. Briels, and W. P. M. van Swaaij, "Discrete particle simulation of bubble and slug formation in a two-dimensional gas-fluidised bed: A hard-sphere approach," Chem. Eng. Sci. **51**, 99 (1996).

[12] M. Chen, K. Kontomaris, and J. B. McLaughlin, "Direct numerical simulation of droplet collisions in a turbulent channel flow. Part I: Collision algorithm," Int. J. Multiphase Flow **24**, 1079 (1999).

[13] S. Sundaram and L. R. Collins, "Numerical considerations in simulating a turbulent suspension of finite-volume particles," J. Comput. Phys. **124**, 337 (1996).

[14] P. Kosinski and A. C. Hoffmann, "Extended hard-sphere model and collisions of cohesive particles," Phys. Rev. E **84**, 031303 (2011).

[15] Y. Yamamoto, M. Potthoff, T. Tanaka, T. Kajishima, and Y. Tsuji, "Large-eddy simulation of turbulent gas-particle flow in a vertical channel: Effect of considering inter-particle collisions," J. Fluid Mech. **442**, 303 (2001).

[16] M. Sommerfeld, "Validation of a stochastic Lagrangian modelling approach for inter-particle collisions in homogeneous isotropic turbulence," Int. J. Multiphase Flow **27**, 1829 (2001).

[17] J. Wang, Q. Shi, Z. Huang, Y. Gu, L. Musango, and Y. Yang, "Experimental investigation of particle size effect on agglomeration behaviors in gas–solid fluidized beds," Ind. Eng. Chem. Res. **54**, 12177 (2015).

[18] D. Jürgens, "Modellierung und simulation der partikelagglomeration in turbulenten, dispersen mehrphasenströmungen," M.S. thesis, Helmut-Schmidt-Universität, 2012.

[19] M. Alletto, "Numerical investigation of the influence of particle–particle and particle–wall collisions in turbulent wall-bounded flows at high mass loadings," Ph.D. thesis, Helmut-Schmidt University, 2014.

[20] N. Almohammed and M. Breuer, "Modeling and simulation of agglomeration in turbulent particle-laden flows: A comparison between energy-based

and momentum-based agglomeration models," Powder Technol. **294**, 373 (2016).

[21] M. Breuer and N. Almohammed, "Modeling and simulation of particle agglomeration in turbulent flows using a hard-sphere model with deterministic collision detection and enhanced structure models," Int. J. Multiphase Flow **73**, 171 (2015).

[22] P. Kosinski and A. C. Hoffmann, "An extension of the hard-sphere particle–particle collision model to study agglomeration," Chem. Eng. Sci. **65**, 3231 (2010).

[23] B. Derjaguin and L. Landau, "Theory of the stability of strongly charged lyophobic sols and of the adhesion of strongly charged particles in solutions of electrolytes," Acta Phys. Chem. URSS **14**, 633 (1941) [Prog. Surf. Sci. **43**, 30 (1993)].

[24] E. J. W. Verwey and J. T. G. Overbeek, *Theory of the Stability of Lyophobic Colloids* (Elsevier, 1948).

[25] M. Alletto and M. Breuer, "One-way, two-way and four-way coupled LES predictions of a particle-laden turbulent flow at high mass loading downstream of a confined bluff body," Int. J. Multiphase Flow **45**, 70 (2012).

[26] M. Breuer and M. Alletto, "Efficient simulation of particle-laden turbulent flows with high mass loadings using LES," Int. J. Heat Fluid Flow **35**, 2 (2012).

[27] D. O. Njobuenwu and M. Fairweather, *Deterministic Modelling of Particle Agglomeration in Turbulent Flow* (Begell House, Inc., Sarajevo, 2015).

[28] M. Bini and W. P. Jones, "Large-eddy simulation of particle-laden turbulent flows," J. Fluid Mech. **614**, 207 (2008).

[29] C. Marchioli, A. Soldati, J. G. M. Kuerten, B. Arcen, A. Tanière, G. Goldensoph, K. D. Squires, M. F. Cargnelutti, and L. M. Portela, "Statistics of particle dispersion in direct numerical simulations of wall-bounded turbulence: Results of an international collaborative benchmark test," Int. J. Multiphase Flow **34**, 879 (2008).

[30] C. Marchioli and A. Soldati, *Reynolds number Scaling of Particle Preferential Concentration in Turbulent Channel Flow* (Springer, Berlin, Heidelberg, 2007).

[31] R. D. Moser, J. Kim, and N. N. Mansour, "Direct numerical simulation of turbulent channel flow up to $Re_\tau = 590$," Phys. Fluids **11**, 943 (1999).

[32] C. M. Rhie and W. L. Chow, "Numerical study of the turbulent flow past an airfoil with trailing edge separation," AIAA J. **21**, 1525 (1983).

[33] H. van der Vorst, "Bi-CGSTAB: A fast and smoothly converging variant of Bi-CG for the solution of nonsymmetric linear systems," SIAM J. Sci. Stat. Comput. **13**, 631 (1992).

[34] D. S. Kershaw, "The incomplete Cholesky-conjugate gradient method for the iterative solution of systems of linear equations," J. Comput. Phys. **26**, 43 (1978).

[35] D. O. Njobuenwu and M. Fairweather, "Simulation of inertial fibre orientation in turbulent flow," Phys. Fluids **28**, 063307 (2016).

[36] U. Piomelli and J. Liu, "Large-eddy simulation of rotating channel flows using a localized dynamic model," Phys. Fluids **7**, 839 (1995).

[37] M. Fairweather and J. P. Hurn, "Validation of an anisotropic model of turbulent flows containing dispersed solid particles applied to gas–solid jets," Comput. Chem. Eng. **32**, 590 (2008).

[38] R. Mei, "An approximate expression for the shear lift force on a spherical particle at finite Reynolds number," Int. J. Multiphase Flow **18**, 145 (1992).

[39] J. M. Tingey, B. C. Bunker, G. L. Graff, K. D. Keeper, A. S. Lea, and D. R. Rector, "Colloidal agglomerates in tank sludge and their impact on waste processing," MRS Online Proc. Libr. **556**, 1315 (1999).

[40] W. J. Stronge, *Impact Mechanics* (Cambridge University Press, 2004).

[41] G. K. El Khoury, P. Schlatter, A. Noorani, P. F. Fischer, G. Brethouwer, and A. V. Johansson, "Direct numerical simulation of turbulent pipe flow at moderately high Reynolds numbers," Flow Turbul. Combust. **91**, 475 (2013).

[42] L.-P. Wang, A. S. Wexler, and Y. Zhou, "Statistical mechanical description and modelling of turbulent collision of inertial particles," J. Fluid Mech. **415**, 117 (2000).

[43] R. Wilson, D. Dini, and B. van Wachem, "A numerical study exploring the effect of particle properties on the fluidization of adhesive particles," AIChE J. **62**, 1467 (2016).

[44] C.-L. Lin and M.-Y. Wey, "The effect of mineral compositions of waste and operating conditions on particle agglomeration/defluidization during incineration," Fuel **83**, 2335 (2004).

[45] G. V. Reddy and S. K. Mahapatra, "Effect of coal particle size distribution on agglomerate formation in a fluidized bed combustor (FBC)," Energy Convers. Manage. **40**, 447 (1999).

[46] M. Dosta, S. Antonyuk, and S. Heinrich, "Multiscale simulation of agglomerate breakage in fluidized beds," Ind. Eng. Chem. Res. **52**, 11275 (2013).

[47] M. Ernst and M. Sommerfeld, "On the volume fraction effects of inertial colliding particles in homogeneous isotropic turbulence," J. Fluids Eng. **134**, 031302 (2012).